Sound & Vibration 2026, 60(4), 4175.
doi: https://doi.org/10.59400/sv4175

Article

Optimization design of fuel tank structure for a certain excavator based on finite element analysis

Bowen Chen, Peigang Jiao*, Guoqing Qi, Yanan Zhang

School of Mechanical Engineering, Shandong Jiaotong University, Jinan 250357, China
* **Corresponding author:** Peigang Jiao, jiaopeigang@163.com

CITATION

Chen B, Jiao P, Qi G, et al. Optimization design of fuel tank structure for a certain excavator based on finite element analysis. Sound & Vibration. 2026; 60(4): 4175. https://doi.org/10.59400/sv4175

ARTICLE INFO

Received: 19 March 2026
Revised: 3 May 2026
Accepted: 8 May 2026
Available online: 22 July 2026

Abstract: This study focuses on the fuel tank of a specific excavator model, employing CATIA for modeling and ANSYS Workbench for finite element analysis. Static strength, modal, and random vibration simulations were performed to address stress concentration, excessive deformation, and resonance risks caused by oil sloshing. An optimized design was proposed and experimentally validated. The original fuel tank was first simplified and modeled using Q235 material. A mesh convergence study determined a 10 mm element size, balancing accuracy and computational efficiency. Static analysis confirmed that maximum stress and deformation met material allowables. Modal analysis revealed a first natural frequency of approximately 67.40 Hz, significantly above the frame's excitation frequency of around 10 Hz, effectively avoiding resonance. Random vibration analysis indicated prominent Y-direction deformation and X-direction stress. An optimization scheme was developed: symmetrically lengthening the transverse anti-slosh baffles and adding rounded stiffening ribs at the bottom. Post-optimization, deformations and stresses decreased markedly in all directions, with X-direction stress reduced by over 60%. Bench strain testing agreed with simulation results to within 91%, verifying the reliability and safety of the optimized structure. Results demonstrate that combining anti-slosh baffles with stiffening ribs significantly enhances vibration resistance, reduces fatigue failure risk, and maintains controllable manufacturing processes and costs. This provides a reusable simulation and optimization methodology for lightweight, durable fuel tank design in construction machinery.

Keywords: vibration characteristics; static strength; modal analysis; reinforcement ribs; wave suppression plate

1. Introduction

Fuel tanks play a crucial role in construction machinery equipment, and relevant national technical specifications have established strict standardization requirements for core indicators such as safety protection, structural strength, and environmental compatibility. However, the currently widely used design scheme for fuel tank anti-wave partitions and reinforced structures has not yet established a complete scientific theoretical support system for key technical aspects such as mechanical performance characteristic analysis and strength-stiffness calculation. Due to the complex working environment of excavators, they frequently experience severe fuel tank vibration under harsh working conditions. Under the impact of oil, the fuel tank is prone to fatigue damage. Therefore, some scholars have conducted a series of studies on the durability of fuel tanks.

Finite element analysis (FEA) has become an indispensable tool for investigating the mechanical behavior of engineering structures across diverse applications, including aerospace, automotive, and civil engineering. Early studies, such as those by Onyibo and Safaei [1] on honeycomb sandwich structures and Muhammad et al. [2] on engine connecting rods, demonstrated the capability of commercial FEA software like ANSYS and ABAQUS to capture the mechanical responses of components under various loading conditions. These works established the feasibility of using numerical methods to evaluate the performance, optimize the design, and improve the fatigue life of engineering parts, providing essential references for subsequent research.

Over time, the scope of FEA applications has expanded to address more complex engineering challenges. Agrawal et al. [3] and Liu et al. [4] extended the use of FEA to the optimization of mechanical transmissions, while Ahiwale et al. [5] and Avikal et al. [6] applied modal and fatigue life analysis to cantilever beams and automotive axles, respectively. These studies not only validated the reliability of FEA in predicting static and dynamic responses but also highlighted its effectiveness in identifying critical stress concentrations and failure modes. Similarly, Chan et al. [7], Cavalheiro et al. [8], and Imran et al. [9] further demonstrated the versatility of FEA in analyzing the static and dynamic characteristics of tools, thick cylinders, and composite plates, offering valuable insights into the behavior of structures under complex boundary conditions.

Recent research has also focused on specific industrial and mechanical components. Tahenni et al. [10], Sreenivasan et al. [11], and Shaikh and Nallasivam [12] used FEA to evaluate the performance of reinforced concrete beams, motorcycle suspensions, and box girder bridges, while Mughal and Bugvi [13] and Idrees et al. [14] investigated the structural integrity and impact response of excavator buckets and car frames. Uğur et al. [15], Sivasuriyan et al. [16], Belhocine and Afzal [17], and Loganathan et al. [18] explored the mechanical properties of honeycomb structures, RC beams, brake discs, and composite materials, respectively, contributing to the development of lightweight and high-performance engineering solutions. Additionally, Khan and Jamshed [19] examined the effect of thermal barrier coatings on tool strength, demonstrating the applicability of FEA in thermal-mechanical coupled analysis.

Despite the extensive use of FEA in engineering practice, several limitations remain. Traditional FEA simulations, while accurate, are often computationally expensive and time-consuming, limiting their application in large-scale parametric studies and real-time prediction scenarios. To address this issue, Al-Haddad et al. [20] proposed a machine learning-based approach combining FEA with SVM and kNN models to accelerate stress prediction in wind tunnel simulations. Their work showed that the SVM model achieved a low RMSE of 2.1% while reducing the computation time from hours to seconds, highlighting the potential of integrating FEA with artificial intelligence to improve computational efficiency. Similarly, Triantafyllou [21] developed the DeepFEA framework, a deep learning-based method for predicting transient FEA solutions, which achieved normalized errors below 3% and an inference speed two orders of magnitude faster than traditional FEA. These studies have opened new avenues for fast and accurate FEA-based predictions, but their applications to specific engineering problems, such as excavator fuel tanks, remain limited.

Furthermore, the optimization of structural components using FEA has been widely explored. Wang et al. [22] conducted a comprehensive analysis of plastic fuel tanks for automobiles, Cadet and Paredes' study [23] on mesh convergence for helical springs, and Firouzi et al.'s research [24] on nonlinear free vibration of beams all demonstrated the effectiveness of FEA in structural optimization and performance improvement. In the field of medical engineering, Pang et al. [25] investigated the effect of opening positions on the fixation accuracy of radiotherapy masks, providing insights for clinical design. However, most existing studies have focused on the static performance of components, and few have comprehensively addressed the vibration characteristics and resonance risk of large-scale engineering structures, such as excavator fuel tanks, under actual working conditions.

In summary, while FEA has been extensively applied to various engineering problems, there is a lack of research focusing on the vibration and structural optimization of excavator fuel tanks, particularly concerning the avoidance of resonance with the vehicle frame and the improvement of fatigue life under complex working conditions. To fill this gap, the present study conducts a comprehensive FEA-based analysis of the fuel tank structure, combining modal analysis, static stress analysis, and structural optimization to improve its performance and reliability.

2. Materials and methods

This article provides an optimized design scheme for the baffle and reinforcement structure of the metal fuel tank of excavators. Because fuel tank damage often occurs under hazardous conditions, the unoptimized model is first analyzed for hazardous conditions, and the environment under hazardous conditions is simulated to obtain data such as pressure, deformation, and mode. At the same time, experiments are designed to verify the reliability of the simulation data. In the case of reasonable simulation data, this paper designs an optimization scheme that combines transverse baffles and reinforcing ribs for parts with high stress and deformation. The fuel tank model was optimized according to this plan, and the optimized fuel tank model was imported into ANSYS again for finite element analysis. The optimized fuel tank was subjected to stress testing, and the results showed that all data of the fuel tank were optimized to varying degrees, proving that the metal fuel tank optimization design scheme proposed in this paper is fully applicable to the fuel tank optimization of construction equipment such as excavators. The flowchart of the optimization design scheme is shown in **Figure 1**.

Based on the specific working conditions of the excavator fuel tank, the model is a hydraulic excavator fuel tank from an enterprise, with dimensions of 750 mm × 600 mm × 950 mm and a plate thickness of 6 mm.

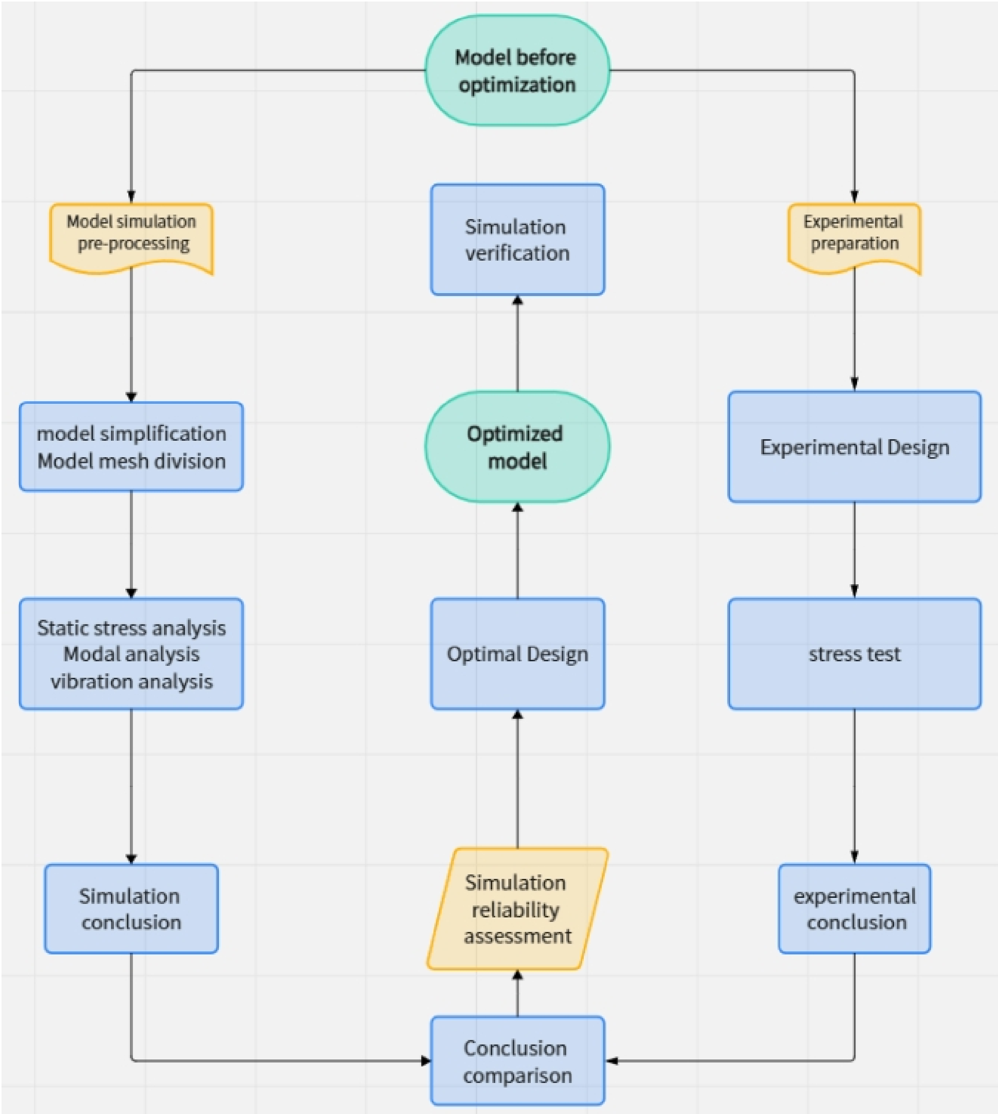

Figure 1. Flow chart of optimization design scheme.

However, in actual simulation experiments, because the model often contains a large number of small features, surfaces, or assemblies, it is more complex to process, which can lead to a significant increase in the number of grids in finite element analysis, significantly increasing the solution time and memory requirements. In order to reduce computational resource consumption and accelerate the calculation speed of finite element analysis, simplified models are used in practical finite element analysis, which can reduce the number of elements/nodes and avoid problems where the model exceeds the computer's memory or processing capacity and cannot be solved. In this fuel tank model, there are many assembly holes on the surface of the tank body for fixing components such as pedals, skid plates, and baffles. Due to the negligible influence of these small mass components on modal analysis in finite element analysis, these components were removed from the optimization model. The simplified model of the fuel tank is shown in **Figure 2**.

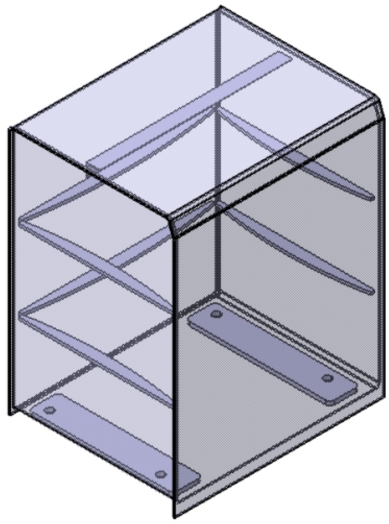

Figure 2. Simplified model of the fuel tank.

The main body of the tank is made of Q235 carbon steel (equivalent to ASTM A36 or EN S235JR), with a nominal yield strength of 235 MPa and an ultimate tensile strength of 375 to 500 MPa. This article selects 420 MPa as the reference value for tensile strength. Set the fuel tank material to Q235 in ANSYS software, and the relevant properties of the material are shown in **Table 1**.

Table 1. Fuel tank material attribute table.

Parameter	Numerical value
modulus of elasticity/MPa	2.10×10^5
Poisson's ratio	0.3
density/(kg/m^3)	7,850
yield strength/MPa	235
tensile strength/MPa	420

In this study, the ultimate tensile strength (UTS) reference value for Q235 steel was set at 420 MPa. While the nominal tensile strength range for this grade spans from 375 to 500 MPa (per GB/T 700-2006 / ISO 630-2), the selection of 420 MPa is justified on the following technical grounds:

(1) Typical upper-bound specification for thin plates: According to the material certification for structural steels with thicknesses ≤ 16 mm—which corresponds to the wall thickness of the excavator fuel tank analyzed herein—the specified tensile strength is typically constrained to an upper limit of 420 MPa in many supplier datasheets. This ensures that the simulation utilizes a minimum guaranteed maximum strength rather than an extreme statistical outlier.

(2) Conservative failure assessment: The finite element analysis aims to evaluate structural integrity under extreme loading (e.g., sloshing and vibration). Adopting a reference value of 420 MPa provides a moderate safety buffer in the plastic collapse assessment. Utilizing the upper extreme of 500 MPa would overestimate the tank's actual load-bearing capacity, whereas using the yield strength (235 MPa) would conflate plastic deformation with ultimate rupture.

(3) Ductility compatibility: Q235 steel exhibits optimal elongation properties (typically > 26%) when the tensile strength is maintained near the 420 MPa threshold. This aligns with the operational requirement for fuel tanks to deform plastically without leakage under accidental overload.

When dividing the fuel tank structure into grids, the number of nodes and elements should be minimized as much as possible to improve calculation speed while ensuring engineering accuracy. Considering the actual working conditions of the excavator, combined with the analysis accuracy, the grid is divided into 10 mm grids with a total of 223,947 grids and 467,718 nodes. The grid division result is shown in **Figure 3**.

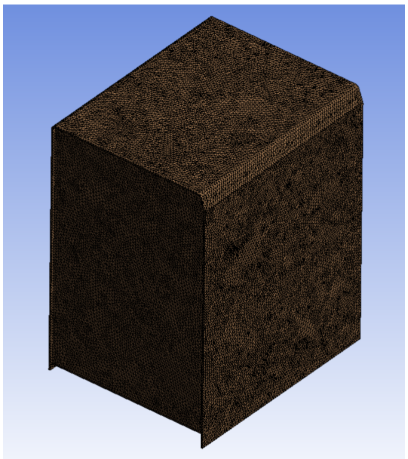

Figure 3. Grid-based model of the fuel tank.

To ensure the reliability and convergence of the finite element simulation results, a mesh convergence study was conducted by comparing three different element sizes: 15 mm, 10 mm, and 5 mm. The results, summarized in **Table 2**, show the maximum stress and deformation under the same load condition for each mesh configuration.

Table 2. Mesh convergence study.

Grid size (mm)	Number of elements	Maximum stress (MPa)	Relative error	Maximum deformation
5	120,156	115.8	+1.1%	0.403
10	223,947	117.19	-	0.407
15	798,458	118.13	−0.8%	0.409

As shown in **Table 2**, refining the mesh from 15 mm to 10 mm led to a 1.1% increase in the maximum stress. When the mesh was further refined to 5 mm, the stress value changed by only 0.8% compared with the 10 mm mesh. The maximum deformation values exhibited a similar trend, converging rapidly and varying by less than 0.5% between the 10 mm and 5 mm configurations.

Considering both numerical accuracy and computational efficiency, the 10 mm mesh size was selected for the subsequent simulations. This configuration provides results that are sufficiently close to the fully converged solution while keeping the total number of elements at approximately 224,000, which ensures a reasonable computational cost.

3. Finite element simulation analysis of fuel tank structure

3.1. Static strength analysis

Static strength analysis is the foundation of engineering mechanics and structural analysis, mainly used to evaluate the bearing capacity and safety of structures or materials under static loads. The static analysis of structures generally assumes that the material has no voids, the mechanical properties are continuously distributed, the properties of the material are the same everywhere, and the mechanical properties of the material are independent of direction. When using the finite element method for object structure analysis, the following matrix can be used to represent the equilibrium equation of structural analysis:

$$[K]\{U\} = \{R\}. \tag{1}$$

Among which, $[K]$ represents the structural stiffness matrix; $\{U\}$ represents the displacement array of structural nodes; $\{R\}$ represents the structural load array.

Calculate the node displacement $\{U\}$ in the above equation, and by calculating, the stress and strain of each unit can be obtained, that is:

$$[\sigma] = [D][B]\{u\}^e, \tag{2}$$

$$[\varepsilon] = [B][u]^{(e)}. \tag{3}$$

Among which, $[D]$ is the elastic matrix of the unit material; $[B]$ is the unit strain matrix.

In this article, the fourth strength theory is used for the static strength verification of excavator fuel tanks, namely:

$$\sigma_{\text{eq}} = \sqrt{\frac{1}{2}[(\sigma_1 - \sigma_2)^2 + (\sigma_2 - \sigma_3)^2(\sigma_3 - \sigma_1)^2]} \leq [\sigma]. \tag{4}$$

The fuel density is 0.85 g/ml, and half of the fuel is converted to a gravity of approximately 1,700 N, with a dynamic load coefficient of 2. The force acting on the bottom of the excavator fuel tank is:

$$F = kmg. \tag{5}$$

Among them, F is the pressure acting on the bottom of the fuel tank; K is the dynamic load coefficient; M is the weight; G is the acceleration due to gravity.

According to formula (5), F is 3,400 N. Under the working conditions of rock excavation, the gravity acceleration of the excavator fuel tank is taken as 3 g. Fixed constraints are applied to the four mounting holes at the bottom of the fuel tank, and the static analysis deformation cloud map of the excavator fuel tank is shown in **Figure 4**, and the stress cloud map is shown in **Figure 5**.

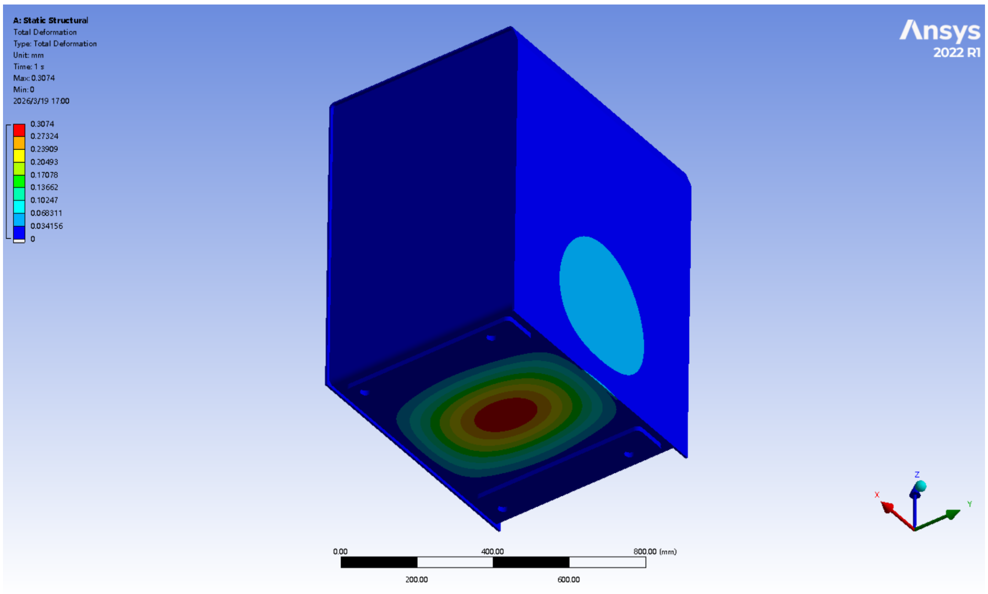

Figure 4. Static analysis deformation cloud map.

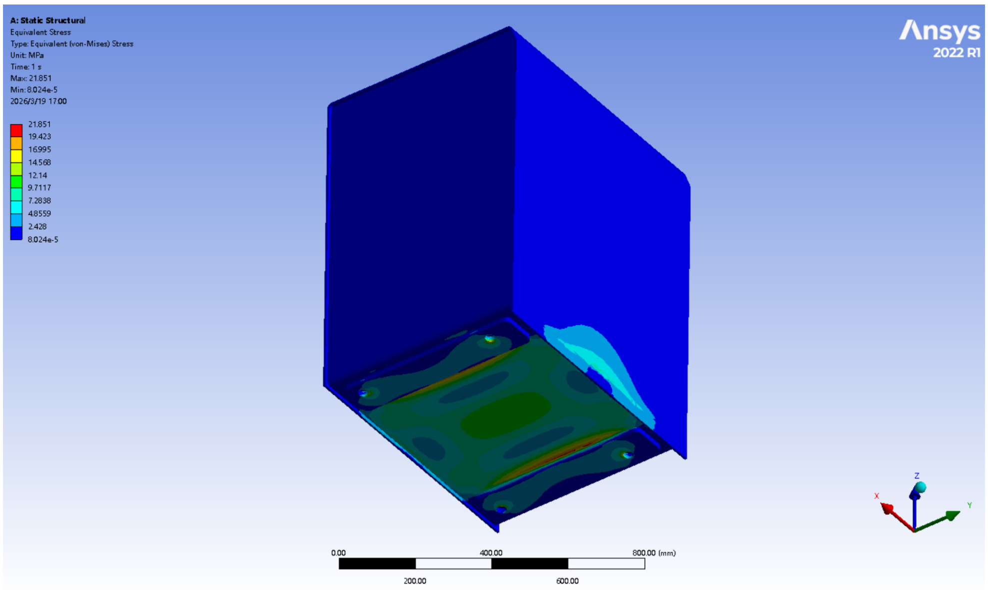

Figure 5. Static analysis stress cloud map.

According to the finite element simulation analysis of the deformation cloud map, it can be seen that during excavation work, the maximum displacement of the fuel tank occurs at the center of the bottom, with a maximum deformation of 0.3074 mm. The maximum stress on the fuel tank occurs at the junction of the bottom and assembly plate, as well as at the four fixed bolt holes, with a maximum stress display of 21.851 MPa. The yield limit of Q235 is 235 MPa, and the allowable stress is 117.5 MPa. Therefore, the stress on the fuel tank of the excavator during rock excavation is much lower than the allowable stress of the material steel.

3.2. Modal analysis

Compared to ordinary vehicle fuel tanks, excavator fuel tanks face more severe vibration, impact, and dynamic load environments. When the fuel tank is subjected to engine, road vibration, or external excitation, if the excitation frequency is close to the natural frequency of the fuel tank or causes a resonance phenomenon, it may cause severe vibration, which may lead to cracking of the fuel tank, fracture of welds, or loosening of connectors, resulting in fuel leakage, abnormal noise, and other problems. Because low-order frequency modes are often the ones that can affect structural safety in engineering, low-order resonance zones should be avoided in design. In order to ensure that the fuel tank of the excavator can maintain its structural reliability, safety, and durability in various complex environments, modal analysis has become particularly crucial.

Modal is mainly expressed through the modal vibration mode and natural frequency of the structure. The natural frequency refers to the natural frequency of the structure during free vibration, and the modal vibration mode is the vibration displacement distribution pattern of each part of the structure at that frequency. The overall differential equation is described as follows:

$$[M]\{x(\ddot{t})\} + [C]\{[X](\dot{t})\} + [K]\{x(t)\} = \{f(t)\}. \tag{6}$$

Among them, $[M]$ represents the mass matrix; $\{f(t)\}$ represents the external excitation matrix that the system is subjected to. $\{[X](\dot{t})\}$ represents the velocity matrix; $[C]$ represents the damping matrix; $[K]$ represents the stiffness matrix; $\{x(\ddot{t})\}$ represents the acceleration matrix;

In the analysis process, the influence of damping effect on the overall vibration characteristics can be ignored, so damping factors were not taken into consideration when modeling structural dynamics. Based on this assumption, the derived system free vibration control equation is expressed as follows:

$$[M]\{x(\ddot{t})\} + [K]\{f(t)\} = \{0\}. \tag{7}$$

The simple harmonic vibration equation is as follows:

$$\{X(\ddot{t})\} = \{\phi\}sin\{wt\}. \tag{8}$$

Among them, w represents the natural frequency; t represents time; $X(t)$ represents the amplitude column vector; $\{\phi\}$ represents node displacement;

By combining the above two equations, we can obtain:

$$([K] - w^2M)\{\phi\} = 0. \tag{9}$$

Solving yields w, Substituting w into the formula yields the characteristic vector value ϕ of the vibration mode.

According to the basic theory of modal analysis, the mode of a structure is independent of the load and is related to the material, structural stiffness, and mass. Therefore, when conducting modal analysis of a fuel tank, only element properties, element materials, and boundary conditions need to be applied to the model. Due to the limitations on boundary conditions, material properties, etc., in static analysis, there is no need for additional requirements in modal analysis. The introduction of the first ten natural frequencies and vibration modes of the fuel tank is shown in **Table 3**, and the vibration mode diagrams of the first four fuel tank structures are shown in **Figure 6**.

Table 3. Description of the first ten natural frequencies and vibration modes.

Modal order	Natural frequency (Hz)	Vibration mode description
1	67.40	First-order local bulging vibration of the right wall panel
2	99.67	Y-direction bending vibration of the fuel tank as a whole
3	125.94	Second-order local bulging vibration of the right wall panel
4	130.47	Overall X-direction translational mode of the fuel tank
5	147.67	Local vibration coupling between the side wall and the bottom plate
6	150.51	Third-order local vibration of the side wall panel
7	159.48	Local bending vibration of the roof
8	169.55	Localized swelling and vibration of the bottom plate
9	179.65	High-order local vibration of side-wall panel
10	195.51	Multi-panel coupled local vibration

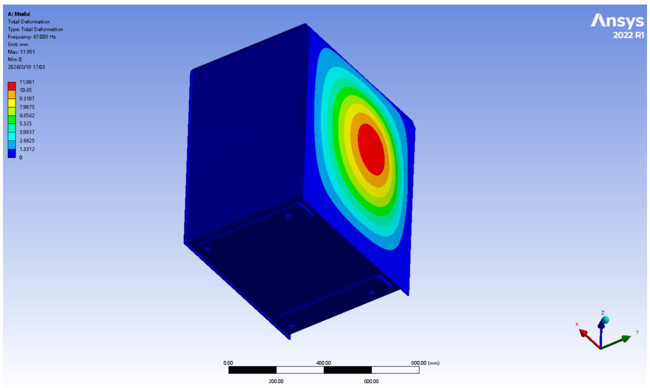

(a) First-order vibration mode diagram

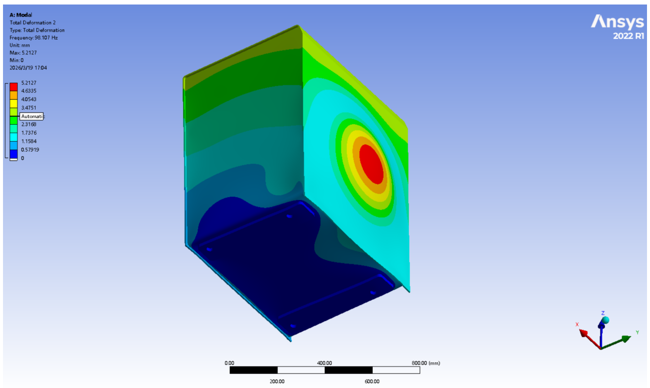

(b) Second-order vibration mode diagram

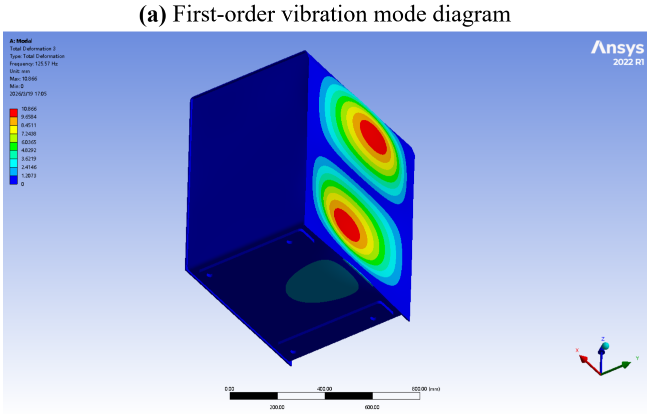

(c) Third-order vibration mode diagram

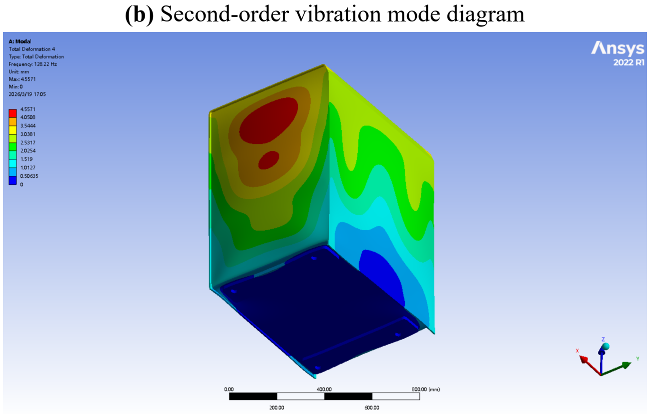

(d) Fourth-order vibration mode diagram

Figure 6. Vibration mode diagram of the fuel tank structure.

According to **Table 3** and **Figure 6**, the first four natural frequencies are 67.40 Hz, 99.67 Hz, 125.94 Hz, and 130.47 Hz, respectively. The first mode is mainly manifested at the center position of the Y-axis side wall of the fuel tank, and the second mode is also mainly manifested at the center position of the Y-axis side wall. But the overall vibration is slightly greater than the first vibration mode. The third vibration mode is mainly manifested on the Y-axis side wall of the fuel tank, but the vibration is concentrated on the upper and lower sides of the center position. The fourth vibration mode is mainly reflected in the X-axis sidewall and the connection between the sidewall and the top.

The environmental vibration test of the excavator frame discussed in this article is conducted in accordance with ISO 20816-1:2016, which is the latest international standard for mechanical vibration measurement and evaluation. The three-axis accelerometer is installed on the rack, and the signal is sampled at 512 Hz for 10 min. The power spectral density (PSD) and frequency response function (FRF) were calculated to determine the natural frequency, which was found to be around 10 Hz. Since the first four natural frequencies of the fuel tank structure are significantly higher than those of the frame, this means that the natural frequency of the fuel tank can completely avoid the excitation caused by excavator vibration.

In order to comprehensively obtain the dynamic characteristics of the fuel tank and provide a reliable modal basis for subsequent random vibration analysis, the first 25 natural frequencies and vibration modes of the fuel tank were also solved. In random vibration analysis, the effectiveness of modal truncation directly affects the accuracy of the results. In engineering, it is usually required that the cumulative effective mass score of the participating modes in each translation direction should not be less than 90% to ensure complete capture of the main dynamic response of the system. **Table 4** lists the cumulative effective mass fraction of fuel tanks in different directions under different modal orders.

Table 4. Cumulative quality scores in different directions.

Modal order	Cumulative mass fraction of X-axis	Cumulative mass fraction of Y-axis	Cumulative mass fraction of Z-axis
4	0.935	0.939	0.163
10	0.960	0.970	0.325
23	0.989	0.994	0.943

According to the calculation results of the modal mass participation coefficient, the cumulative effective mass scores in the X and Y directions reached over 90% of the truncation criteria in the first 4 and 10 modes, respectively. However, the mass participation in the Z direction showed obvious delay characteristics, and it was not until the 23rd mode that its cumulative effective mass score reached 91.2%, meeting the modal truncation requirements.

Further analysis of the vibration modes reveals that in the first 22 modes, the effective mass in the Z direction is dispersed by the local bending vibration and overall torsional mode of the fuel tank wall panel, and no significant overall translational mode is observed. Until the 23rd mode, the rigid translational component of the fuel tank in the Z direction is fully excited, dominating the mass participation in that direction.

To ensure that the modal truncation of the three translational directions in the subsequent random vibration analysis meets the 90% standard, this analysis extends the solved modal order to the first 25 orders. At this point, the cumulative effective mass scores in the X, Y, and Z directions all exceed 90%, providing a complete modal basis for subsequent dynamic response analysis.

3.3. Vibration analysis of fuel tank

During the operation of excavators, various components often vibrate significantly, such as engine vibration, hydraulic system pulsation, bucket excavation, hammer operation, and driving system vibration. Under these vibrations, the oil in the fuel tank may shake and cause structural damage to the tank. Vibration analysis of fuel tanks can not only provide safety assurance for drivers, but also reduce maintenance costs, provide a theoretical basis for fuel tank production and processing, and accumulate key data for the next generation of products.

To simulate the random vibration load borne by the excavator fuel tank during actual operation, combined with the actual installation environment of the excavator fuel tank, the power spectral density (PSD) curve of the foundation acceleration excitation was defined, as shown in **Figure 7**. The excitation frequency range is set to 0–200 Hz, covering the first 25 natural frequencies of the fuel tank to ensure the effectiveness of modal truncation. The PSD curve reaches its peak near 100 Hz, which coincides with the main vibration frequencies of the engine and walking mechanism during excavator operation, and can truly reflect the vibration load characteristics borne by the tank.

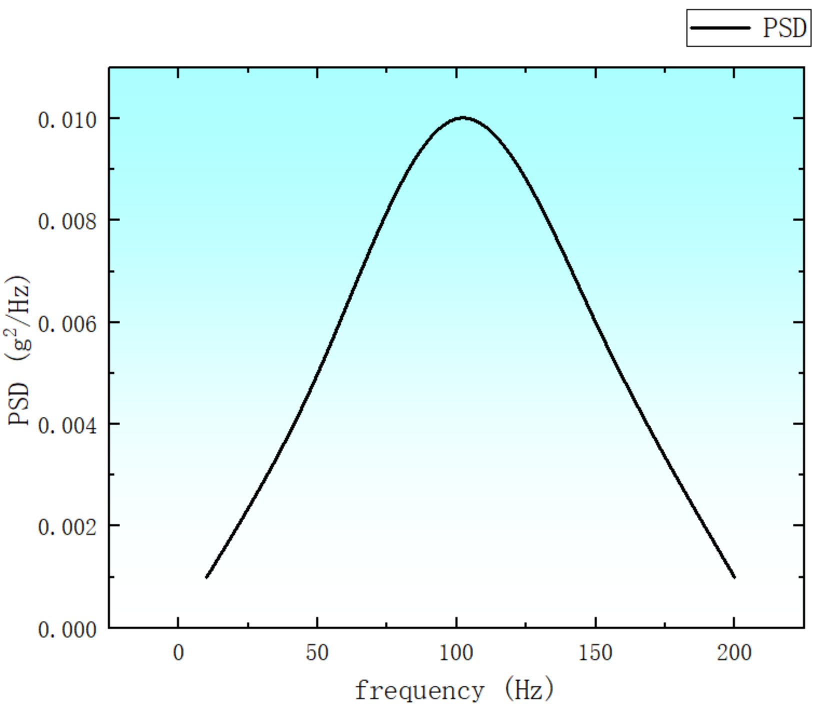

Figure 7. PSD spectrum.

In order to further investigate the influence and characteristics of fuel on the vibration of the fuel tank, we imported the model of the fuel tank into ANSYS Workbench software and conducted vibration simulation experiments in three different directions: the X-axis, Y-axis, and Z-axis based on modal analysis. The deformation cloud map is shown in **Figure 8**, and the stress cloud map is shown in **Figure 9**.

According to **Figures 8** and **9**, the total deformation of the fuel tank in the X-axis direction is 0.407 mm, and the maximum stress is 117.19 MPa. The total deformation of the fuel tank in the Y-axis direction is 1.187 mm, and the maximum stress is 94.48 MPa. The total deformation of the fuel tank in the Z-axis direction is 0.080 mm, and the maximum stress is 14.235 MPa.

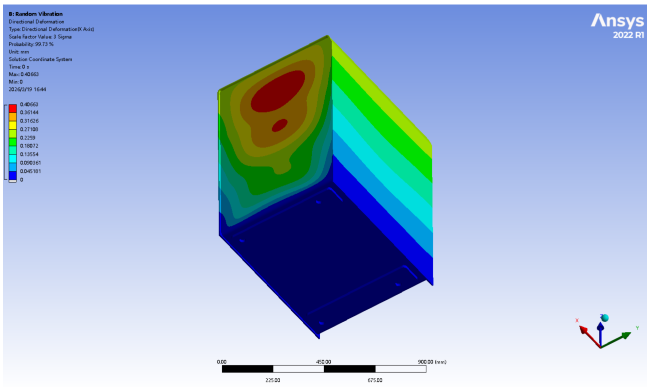

(a) X-axis total deformation diagram

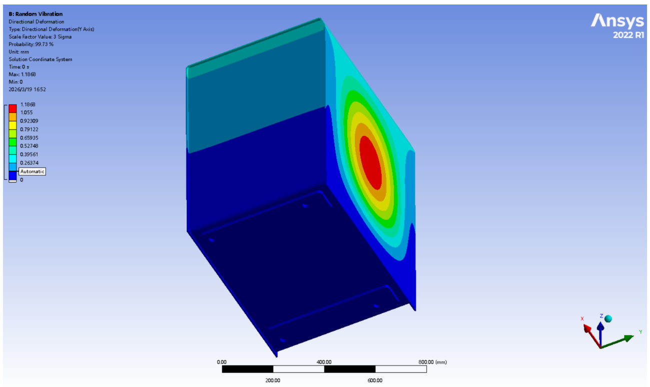

(b) Y-axis total deformation diagram

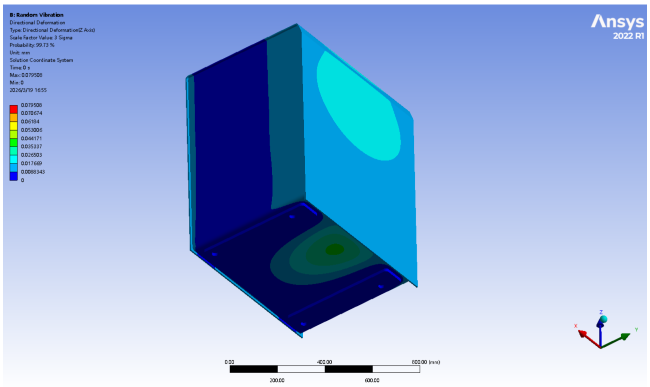

(c) Z-axis total deformation diagram

Figure 8. Cloud map of fuel tank deformation.

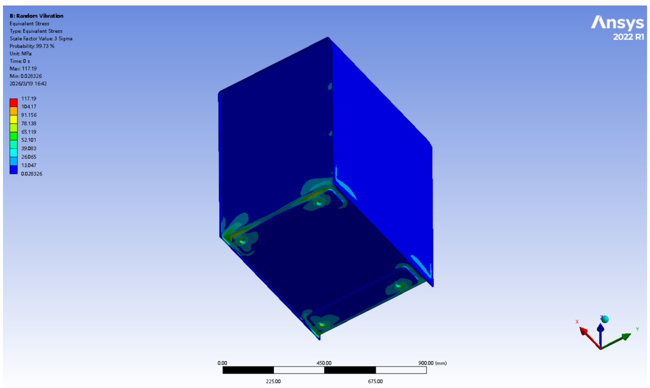

(a) X-axis stress cloud map

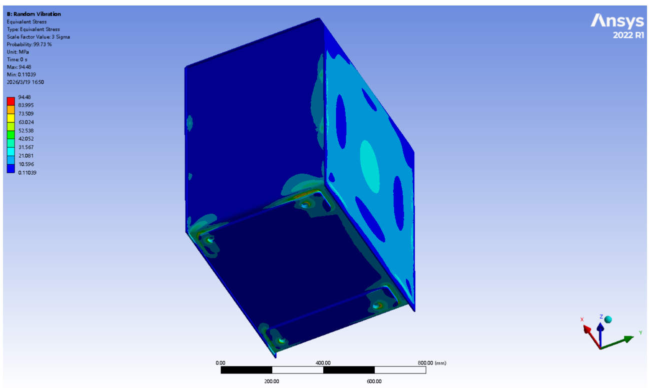

(b) Y-axis stress cloud map

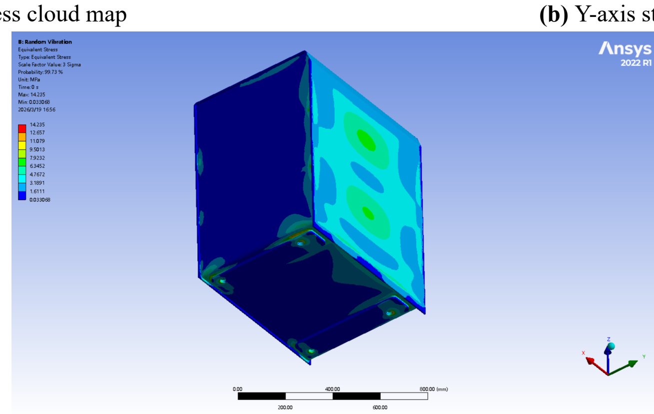

(c) Z-axis stress cloud map

Figure 9. Equivalent stress cloud map of the fuel tank.

To optimize the excavator fuel tank based on simulation analysis data, the transverse wave suppression plate is first designed symmetrically. The transverse wave suppression plate is a sheet metal part that is prone to deformation due to stress concentration before optimization. During optimization, it was symmetrically designed on the original design scheme and extended 16 mm on both sides, allowing both ends to be welded to the inner wall of the fuel tank to increase stability. The design of the wave suppression board before and after optimization is shown in **Figure 10**.

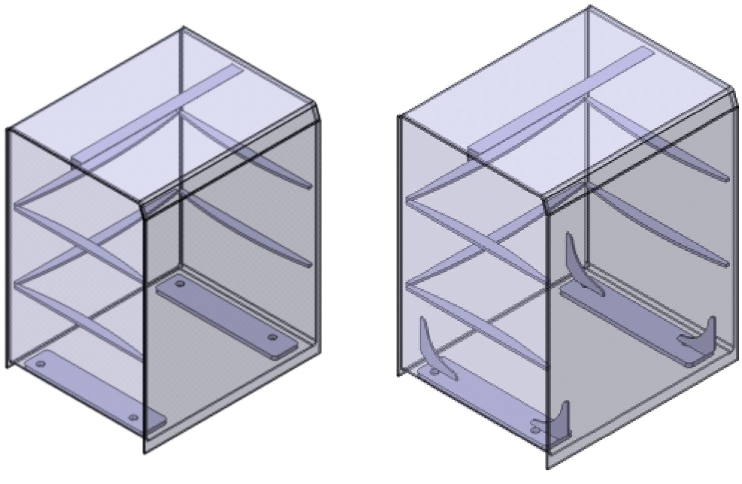

(a) Before optimization **(b)** Optimized

Figure 10. Horizontal wave suppression plate of the fuel tank before and after optimization.

In response to the issue of high stress at the installation hole at the bottom of the fuel tank, a reinforcement rib installation plan has been adopted. Four transverse reinforcing ribs are installed at the bottom of the fuel tank. The reinforcing rib is close to the inner wall and has a chamfer at the bend to facilitate oil flow and prevent stress concentration. The overall edge adopts rounded corner technology, enhancing impact resistance, simplifying processing technology, and avoiding certain processing risks. The design before and after reinforcement optimization is shown in **Figure 11**.

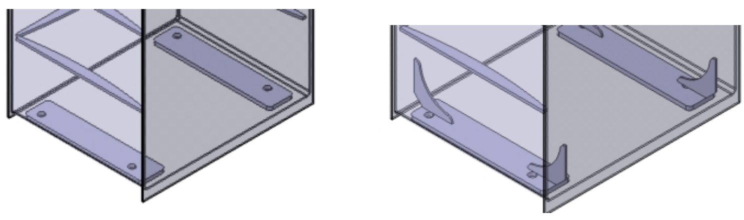

(a) Before optimization **(b)** Optimized

Figure 11. Reinforcement optimization plan.

Import the optimized fuel tank model into the Model and Random Vibration modules of ANSYS Workbench, and obtain vibration deformation cloud maps and stress cloud maps in the X, Y, and Z directions of the optimized fuel tank under the same constraints and environment as the pre-optimization simulation experiment, as shown in **Figures 12** and **13**.

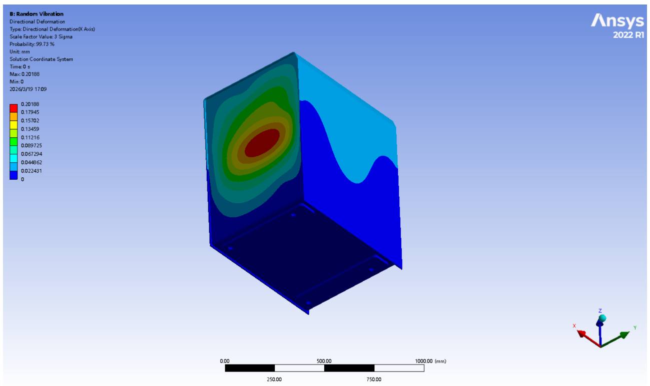

(a) X-axis deformation cloud map

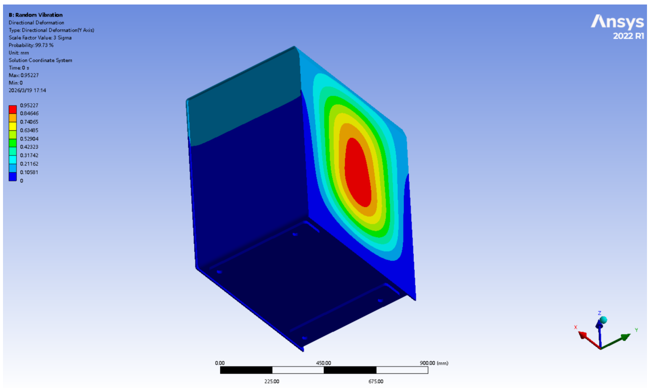

(b) Y-axis deformation cloud map

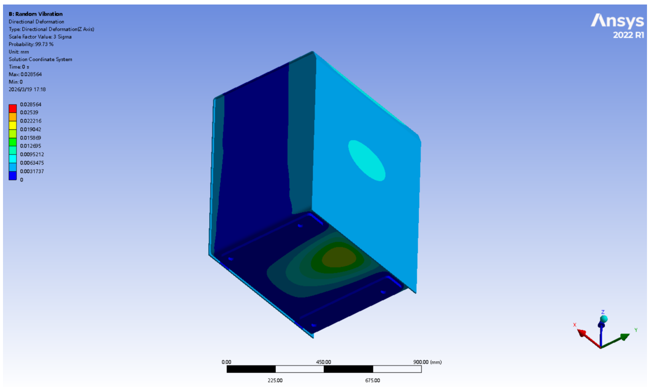

(c) Z-axis deformation cloud map

Figure 12. Optimized deformation cloud map in all directions.

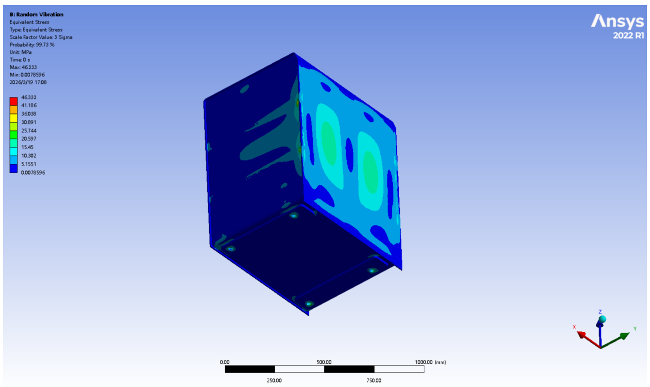

(a) X-axis stress cloud map

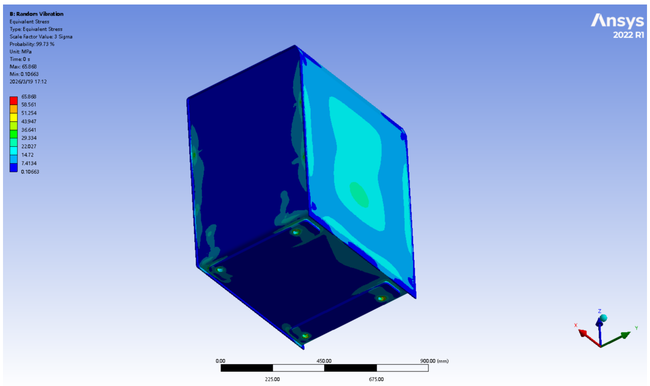

(b) Y-axis stress cloud map

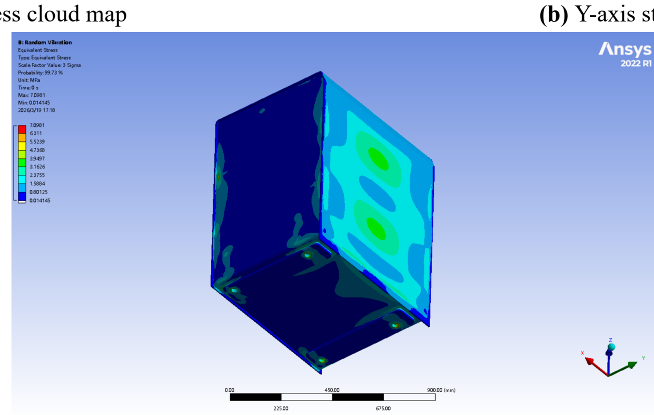

(c) Z-axis stress cloud map

Figure 13. Stress cloud map in all directions after optimization.

According to **Figures 12** and **13**, the total deformation of the optimized fuel tank in the X-axis direction is 0.202 mm, and the maximum stress is 46.333 MPa. The total deformation of the fuel tank in the Y-axis direction is 0.952 mm, and the maximum stress is 65.868 MPa. The total deformation of the fuel tank in the Z-axis direction is 0.029 mm, and the maximum stress is 7.098 MPa. The comparison results before and after optimization are shown in **Table 5**.

Table 5. Comparison of vibration analysis data before and after fuel tank optimization.

	Before optimization		Optimized	
	Deformation/mm	**Stress/MPa**	**Deformation/mm**	**Stress/MPa**
X-axis	0.407	117.19	0.202	46.333
Y-axis	1.187	94.48	0.952	65.868
Z-axis	0.080	14.235	0.029	7.098

From **Table 5**, it can be clearly seen that the optimized fuel tank has been greatly optimized in terms of deformation and stress on all axes, with the most significant reduction in stress on the X-axis and Y-axis. From this, it can be seen that in this paper, we used optimization design methods for wave suppression plates and reinforcement ribs, which can effectively reduce the negative effects of fuel shock on the fuel tank during excavator operation.

In order to verify the authenticity of the simulation and the rationality of the optimized design, the optimized metal fuel tank of the excavator will be experimentally verified. According to the simulation results, the maximum stress point of the excavator's metal fuel tank is near the four installation holes at the bottom. Therefore, the design experiment places four strain gauges near the four installation holes to test the actual stress situation at the four positions. **Figure 14** shows the theoretical placement position of the strain gauge, and **Figure 15** shows the actual placement position of the strain gauge.

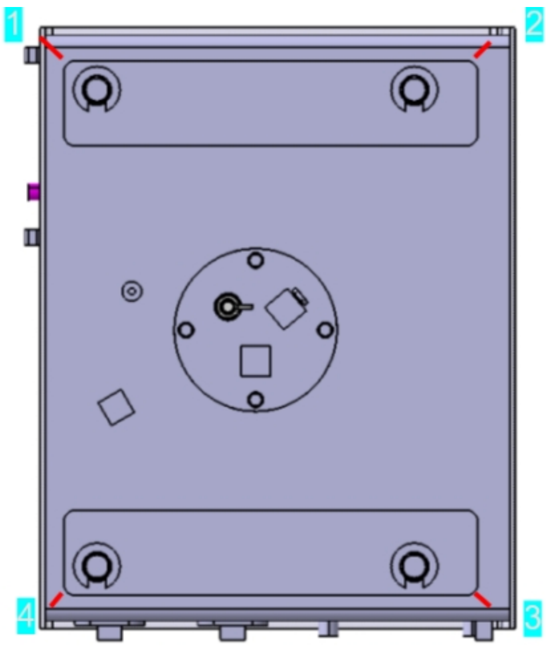

Figure 14. Theoretical placement position of strain gauges.

(a) Strain gauges 2 and 4 **(b)** Strain gauges 1 and 3

Figure 15. Actual placement position of strain gauges.

Strain gauges are placed at the four corner mounting points of the fuel tank (**Figure 14**) to monitor the critical stress concentration under vibration loads. The coordinates are based on the fuel tank dimensions of 600 mm × 750 mm, which are (20, 730), (580, 730), and (580, 20) mm, respectively.

In addition, the installation error of strain gauges was taken into account in the experimental design. The position error is controlled within ±2 mm, and the angle alignment error relative to the principal stress direction is limited to ±5°. The bonding and curing processes are carried out according to standard procedures, resulting in an estimated strain transfer error of less than ±2%. Based on these factors, the overall uncertainty of strain measurement is evaluated to be within ±5%, which is acceptable for engineering validation.

4. Results

After multiple experiments and tests, obvious invalid data were excluded. Some experimental test data are shown in **Table 6**:

Table 6. Actual stress measurement of strain gauge 1–4 under stonework operation.

	Stonework 1		**Stonework 2**		**Stonework 3**	
	Max	**Min**	**Max**	**Min**	**Max**	**Min**
Strain gauge 1	70.1	−71	66.5	−65	66.6	−65.2
Strain gauge 2	75.6	−70.8	69.9	−66.2	66.4	−68.7
Strain gauge 3	77.1	−68.9	69.5	−64.9	69.5	−67.8
Strain gauge 4	70.7	−68.5	68.5	−69.8	70.3	−70.1

4.1. Experimental stress distribution under stonework conditions

Physical experiments were conducted on the optimized fuel tank under stonework operating conditions to validate the finite element simulation data. Strain gauges were strategically positioned at the four mounting holes at the bottom of the tank, which were identified as critical stress concentration points during the simulation phase. **Table 6** presents the maximum and minimum stress values recorded across three distinct stonework test runs.

In the first test run (Stonework 1), the maximum stress was recorded at Strain gauge 3, reaching 77.1 MPa, while Strain gauge 2 showed a peak of 75.6 MPa. During the second run (Stonework 2), the stress distribution shifted slightly, with Strain gauge

2 registering the highest value of 69.9 MPa. In the third run (Stonework 3), Strain gauge 4 exhibited the peak stress of 70.3 MPa. Across all tests, the measured stress values remained within the range of 64.9 MPa to 77.1 MPa. The variability in the location of the maximum stress point suggests dynamic load shifts during operation, yet the magnitude of stress remained consistent with the predicted reduction trends observed in the simulation.

4.2. Correlation between simulation and experimental data

The experimental data yielded an overall average maximum stress of approximately 72.4 MPa across the four monitoring points. This figure was compared against the simulated maximum stress of 65.868 MPa obtained from the ANSYS Random Vibration module for the optimized model. The comparison reveals a coincidence degree of roughly 91%, indicating a high level of accuracy in the simulation model. The experimental results confirm that the optimized structure effectively maintains stress levels well below the yield limit of the Q235 material (235 MPa) and the allowable stress (117.5 MPa). Specifically, the optimization measures—symmetric extension of transverse wave suppression plates and the addition of bottom reinforcement ribs—resulted in a significant reduction in stress compared to the pre-optimization simulation values, where stresses in the X-axis reached as high as 117.19 MPa.

5. Discussion

5.1. Significance of structural optimization strategies

The findings demonstrate that the proposed optimization strategy significantly mitigates the structural risks associated with fuel sloshing in excavators. By symmetrically extending the transverse wave suppression plates and adding chamfered reinforcement ribs at the bottom, the study successfully addressed the primary failure mechanisms: stress concentration at mounting holes and excessive deformation of side walls. The reduction in maximum stress by over 60% in the X-axis (from 117.19 MPa to 46.33 MPa in simulation) and substantial decreases in the Y and Z axes highlight the effectiveness of targeting specific geometric weaknesses. This is particularly significant given the harsh working environments of excavators, where fatigue failure due to continuous vibration and dynamic loading is a primary concern.

5.2. Impact on safety and design methodology

The high correlation between the finite element analysis (FEA) predictions and the physical experimental results validates the use of ANSYS Workbench as a reliable predictive tool for fuel tank design in construction machinery. This alignment suggests that simulation-driven design can drastically reduce the reliance on costly and time-consuming trial-and-error prototyping. Furthermore, ensuring that the natural frequencies of the tank (ranging from 67.12 Hz to 127.79 Hz) remain distinct from the excitation frequency of the excavator frame (~10 Hz) prevents resonance, thereby enhancing the long-term durability and operational safety of the equipment. The successful application of these principles confirms that passive structural modifications can serve as a robust countermeasure against dynamic loads without necessitating heavier materials or complete redesigns.

5.3. Broader context for the construction machinery industry

While this study focused on a specific excavator model, the methodology provides a scalable framework for the broader construction equipment industry. The integration of wave suppression plates with reinforced rib structures can be adapted for other heavy machinery, such as loaders and bulldozers, which face similar dynamic loading challenges. The success of this approach suggests that systematic finite element optimization, verified by targeted strain gauge testing, should become a standard practice in the design of fluid-carrying components. This shift toward predictive engineering supports the industry's move toward lighter, more efficient, and safer machinery that meets increasingly stringent safety and environmental regulations.

5.4. Feasibility analysis of the optimized design

The optimized fuel tank structure adopts symmetrical transverse baffles with four rounded ribs at the bottom. From a manufacturing perspective, these modifications introduce a controllable increase in production complexity and material costs, as they only require fine-tuning of existing bending and welding processes without the need for new tools or molds. The estimated additional material cost is about 3–5% of the total raw material cost. However, the maximum stress (exceeding 60% in the X-axis and 30% in the Y-axis) significantly improved the structural durability and fatigue life of the fuel tank. Overall, the proposed design achieves a favorable cost-benefit trade-off, with a slight increase in cost offset by a significant improvement in vibration resistance, making it suitable for practical industrial applications.

5.5. Potential for further improvement in Y-axis stiffness

In this article, the Y-axis deformation of the fuel tank decreased from 1.187 mm to 0.952 mm, representing a reduction of approximately 20%, which is not as significant as the improvement in the X-axis. This is mainly because the current optimization scheme focuses on increasing the bending stiffness in the X-axis direction through transverse baffles, while the vertical stiffness of the sidewall in the Y-axis direction has not been significantly improved. Although the deformation in the Y-axis direction still meets the design requirements, the reviewer's suggestions are of great value for further structural optimization. In future work, it will be considered to add vertical reinforcement ribs on the side walls or adjust the direction of the baffle to improve the stiffness distribution in the Y-axis direction, thereby achieving more balanced structural performance in all directions.

6. Conclusion

The interpretation of the study's outcomes confirms that the structural integrity of excavator fuel tanks under hazardous working conditions is critically dependent on the management of dynamic loads caused by fuel sloshing. The research establishes that passive structural modifications, specifically the geometric optimization of internal baffles and the strategic placement of reinforcement ribs, serve as an effective countermeasure against stress concentration and excessive deformation.

The high degree of agreement between the finite element predictions and physical experimental data underscores the validity of the simulation-driven design approach. It indicates that the observed improvements in safety margins are not merely theoretical but are reproducible in real-world operational scenarios. Consequently, the implementation of these optimized features transforms the fuel tank from a potential failure point into a robust component capable of withstanding severe vibrational environments.

Ultimately, this work signifies a shift towards more predictive and precise engineering in the construction equipment sector. By demonstrating that targeted structural enhancements can drastically reduce stress peaks without necessitating a complete redesign or heavier materials, the study offers a pathway for manufacturing lighter, safer, and more cost-effective machinery. The principles derived here extend beyond the specific case study, offering a foundational logic for future innovations in the durability analysis of mobile hydraulic systems.

Author contributions: Conceptualization, BC; methodology, BC; software, BC; validation, PJ and GQ; formal analysis, YZ; investigation, PJ; resources, YZ; data curation, BC; writing—original draft preparation, BC; writing—review and editing, BC; visualization, PJ; supervision, GQ; project administration, PJ; funding acquisition, PJ. All authors have read and agreed to the published version of the manuscript.

Funding: This study is funded by the Key R&D Program of Shandong Province (Key Technology Research for the Development of an All-Terrain Intelligent Orchard Platform, Project No. 2019GNC106032) and the Science and Technology Plan Project of Shandong Provincial Department of Transportation (Structural Design and Thermal Stress Simulation Analysis of New Heat Dissipation Reinforcement Brake Disc, Project No. 2023B88).

Institutional review board statement: Not applicable.

Informed consent statement: Not applicable.

Data availability statement: All datasets used and generated in this study are available from the corresponding author on reasonable request.

Conflict of interest: The authors declare no conflict of interest.

AI use statement: During the preparation of this manuscript, the authors used ChatGPT solely for language refinement. No AI tools were used for data analysis, interpretation, or generation of scientific content. All outputs were critically reviewed and edited by the authors. The authors take full responsibility for the integrity and accuracy of the work.

References

1. Onyibo EC, Safaei B. Application of finite element analysis to honeycomb sandwich structures: a review. Reports in Mechanical Engineering. 2022; 3(1): 283–300. Available online: https://www.rme-journal.org/index.php/asd/article/view/84
2. Muhammad A, Ali MAH, Shanono IH. Finite Element Analysis of a connecting rod in ANSYS: An overview. IOP Conference Series: Materials Science and Engineering. 2020; 736(2): 022119. doi: 10.1088/1757-899X/736/2/022119
3. Agrawal AP, Ali S, Rathore S. Finite element stress analysis for shape optimization of spur gear using ANSYS. Materials Today: Proceedings. 2022; 64: 1147–1152. doi: 10.1016/j.matpr.2022.03.404
4. Liu Y, Gao X, Huang H, et al. Design and Finite Element Analysis of Reducer Housing Based on ANSYS. Symmetry. 2025; 17(10): 1663. doi: 10.3390/sym17101663
5. Ahiwale D, Madake H, Phadtare N, et al. Modal analysis of cracked cantilever beam using ANSYS software. Materials Today: Proceedings. 2022; 56: 165–170. doi: 10.1016/j.matpr.2022.01.055
6. Avikal S, Bisht A, Sharma D, et al. Design and fatigue analysis of front axle beam of a heavy duty truck using ansys. Materials Today: Proceedings. 2020; 26: 3211–3215. doi: 10.1016/j.matpr.2020.02.901
7. Chan TC, Ullah A, Roy B, et al. Finite element analysis and structure optimization of a gantry-type high-precision machine tool. Scientific Reports. 2023; 13(1): 13006. doi: 10.1038/s41598-023-40214-5
8. Cavalheiro FN, Cabaleiro M, Conde B, et al. Clamp-based steel connections for structural reusability: Experimental and finite element analysis in the elastic range. Structures. 2025; 75: 108767. doi: 10.1016/j.istruc.2025.108767
9. Imran M, Khan R, Badshah S. Experimental, analytical, and finite element vibration analyses of delaminated composite plates. Scientia Iranica. 2019; 28(1). doi: 10.24200/sci.2019.51508.2223
10. Tahenni T, Bouziadi F, Boulekbache B, et al. Experimental and nonlinear finite element analysis of shear behaviour of reinforced concrete beams. Structures. 2021; 29: 1582–1596. doi: 10.1016/j.istruc.2020.12.043
11. Sreenivasan M, Kumar MD, Krishna R, et al. Finite element analysis of coil spring of a motorcycle suspension system using different fibre materials. Materials Today: Proceedings. 2020; 33: 275–279. doi: 10.1016/j.matpr.2020.04.051
12. Shaikh MF, Nallasivam K. Static analysis of box-girder bridge under the influence of Indian railway vehicle loading using ANSYS finite element model. Advances in Bridge Engineering. 2022; 3(1): 25. doi: 10.1186/s43251-022-00076-9
13. Mughal KH, Bugvi SA, et al. Numerical Evaluation of Contemporary Excavator Bucket Designs using Finite Element Analysis. Jurnal Kejuruteraan. 2021; 33(3): 579–591. doi: 10.17576/jkukm-2021-33(3)-18
14. Idrees U, Ahmad S, Shah IA, et al. Finite element analysis of car frame frontal crash using lightweight materials. Journal of Engineering Research. 2023; 11(1): 100007. doi: 10.1016/j.jer.2023.100007
15. Uğur L, Duzcukoglu H, Sahin OS, et al. Investigation of impact force on aluminium honeycomb structures by finite element analysis. Journal of Sandwich Structures & Materials. 2020; 22(1): 87–103. doi: 10.1177/1099636217733235
16. Sivasuriyan A, Vijayan DS, Sankaran N, et al. Finite element analysis of RC beams using static experimental data to predict static and dynamic behaviors. Scientific Reports. 2024; 14(1): 31238. doi: 10.1038/s41598-024-82537-x
17. Belhocine A, Afzal A. Computational finite element analysis of brake disc rotors employing different materials. Australian Journal of Mechanical Engineering. 2022; 20(3): 637–650. doi: 10.1080/14484846.2020.1733175
18. Loganathan TG, Vinoth Kumar K, Madhu S. Flexural and fatigue of a composite leaf spring using finite element analysis. Materials Today: Proceedings. 2020; 22: 1014–1019. doi: 10.1016/j.matpr.2019.11.265
19. Khan SU, Jamshed W. Finite Element Analysis and Wear Rate Analysis of Nano Coated High Speed Steel Tools for Industrial Application. Babylonian Journal of Mechanical Engineering. 2023; 1(1): 12–19. doi: 10.58496/BJME/2023/002
20. Al-Haddad L, Jaber A, Ibraheem L, et al. Enhancing Wind Tunnel Computational Simulations of Finite Element Analysis Using Machine Learning-Based Algorithms. Engineering and Technology Journal. 2023; 42(1): 1–9. doi: 10.30684/etj.2023.142873.1552
21. Triantafyllou G, Kalozoumis PG, Dimas G, et al. DeepFEA: Deep learning for prediction of transient finite element analysis solutions. Expert Systems with Applications. 2025; 269: 126343. doi: 10.1016/j.eswa.2024.126343
22. Wang W, Zhang Z, Liu G, et al. Simulation study on the vibration durability test of an automotive plastic fuel

tank based on fluid–structure coupling. Proceedings of the Institution of Mechanical Engineers, Part D: Journal of Automobile Engineering. 2025; 239(4): 1240–1250. doi: 10.1177/09544070231217553

23. Cadet G, Paredes M. Convergence analysis and mesh optimization of finite element analysis related to helical springs. Mechanics & Industry. 2024; 25: 22. doi: 10.1051/meca/2024018
24. Firouzi N, Lenci S, Amabili M, et al. Nonlinear free vibrations of Timoshenko–Ehrenfest beams using finite element analysis and direct scheme. Nonlinear Dynamics. 2024; 112(9): 7199–7213. doi: 10.1007/s11071-024-09403-3
25. Pang G, Lu Y, Xu Y, et al. The investigation of opening modes of head and neck thermoplastic mask for radiotherapy based on finite element analysis. Radiation Oncology. 2025; 20(1): 64. doi: 10.1186/s13014-025-02648-1